Journal of New Technology and Materials (JNTM)
J. New Technol. Mater.
Vol. 08, N°01 (2018)126-138

OEB Univ. Publish. Co.

Optoelectronic and magnetic properties of the ortho-perovskite $GdRuO_3$ using DFT+U with spin-orbit coupling: predictive study

A. Labdelli[a]*, S. Meskine[a], A. Boukortt[a] and R. Khenata[b]

[a]Elaboration, Characterization Physico-Mechanics of Materials and Metallurgical Laboratory ECP3M, Faculty of Sciences and Technology, Abdelhamid Ibn Badis University of Mostaganem, Mostaganem, Algeria
[b]Laboratory of Quantum Physics of Matter and Mathematical Modeling (LPQ3M) University of Mascara, Mascara 29000, Algeria

Corresponding author, email: abbes.labdelli@univ-mosta.dz

Received date: Apr. 11, 2018; revised date: May 27, 2018; accepted date: June 08, 2018

Abstract

We have investigated the structural, magnetic, and optoelectronic properties of the ortho-perovskite $GdRuO_3$ using the accurate full-potential linearized augmented plane wave (FP-LAPW) method based on the density functional theory (DFT). The generalized gradient approach (GGA) was used to treat the exchange and correlation potential while the GGA+U was found to correct the deficiencies of the GGA. The Hubbard U was taken to be 6 eV (an experimental and theoretical value).Besides, the modified Becke-Johnson (mBJ) exchange potential was also adopted along in combination with the GGA+U approach (mBJ+U) to enhance the description of the electronic structure. The A-type antiferromagnetic phase of the compound $GdRuO_3$ is more stable than the other magnetic phases. The calculated magnetic moments in $GdRuO_3$ were found to emerge especially from the Gd-4f states electrons. The different values semiconductor gap obtained respectively with GGA+U and mBJ+U were 1.4269 eV and 2.9039 eV. These values were increased at 3.5355 eV with the investigation of spin-orbit coupling effects (SOC) on the electronic structure. The mBJ+U+SOC approximation was also used to calculate the optical properties by determining the complex dielectric function from which are derived the other parameters.

Keywords: Perovskite; $GdRuO_3$; Antiferromagnetic; mBJ correction; spin-orbits coupling

1. Introduction

Recently, the perovskite materials with ABO_3 formula have been extensively studied because of their many technological applications. They are investigated in several technological domains. They are considered as sensors and catalysts [1], supraconductors [2,3],multiferroic [4], colossal magnetoresistance [5,6],ferromagnetic and half-metallic [7-10], ceramic fuel cells [11], transition metal-insulator, piezoelectricity/ferroelectricity [12-16], dielectrics [17],semiconductors [18] and other properties[19,20].The ideal cubic structure ABO_3 formula is adopted by most perovskite oxides, where the "A" cation is divalent and the "B" cation is tetravalent[21]. The general view of the perovskite lattice is that it consists of small "B" cations within oxygen octahedra, and larger "A" cations which are 12-fold coordinated by oxygen. The structure-types of these materials has a large diversity of derivative: cubic, orthorhombic, hexagonal and rhombohedra. This is an important factor which increases their physical properties[22]. There are many physical properties studies of perovskites,both theoretically and experimentally [6,23].Transition metal-based perovskites like $CaRuO_3$, $SrFeO_3$, $SmAlO_3$ .... have been widely elaborated and compared to other perovskites due to their half metallic properties[24-26]which are the basic properties of a material forexploitation the technique spin-electronic(spintronic) [27] devices. Recently, intense research on experimental and theoretical fronts focuseson perovskite oxides combining in the same time rare earth and transition metal elements which have been greatly investigated due to their wide variety in physical phenomena [28]. We can cite many examples as the ortho-ferrites ($GdFeO_3$) [29], rare earth aluminate ($SmAlO_3$)[30] and the orthoRuthenate perovskites ($LnRuO_3$ where Ln = rare earth element)[31]besides, they have done the essential part of our work. Ruthenium-oxide perovskites have a wide range of unusual physical properties [32]: band ferromagnetism in $SrRuO_3$[33] and localized magnetism in Ca_2RuO_4[34] are two illustrative examples. It is known that Ruthenium often adopts oxidation states between +4 and+7 in oxides. The very common is Ruthenium(IV) which is found in $ARuO_3$ perovskites(A = Ca, Sr,and Ba) [33, 35, 36], contrary to oxides of ruthenium in the +2 and +3 states, they stay almost unknown, but recently ruthenium(II) oxide $SrFe_{0.5}Ru_{0.5}O_2$ was synthesized by the topochemical reduction of $SrFe_{0.5}Ru_{0.5}O_3$[37].Additionally, a wide series of new $LnRuO_3$ (Ln = Nd, Sm, Eu, Gd,Tb, Dy, Ho and Y) perovskites has been synthesized too at high pressure and shows that Ru^{3+}canalso be isolated in perovskites[38]. An orthorhombic Pnma perovskite superstructure is adopted by the $LnRuO_3$ materials with tetragonal compression of the RuO_6 octahedra [38]. This distortion, and the observed narrow band gap semiconductivity and small

effective-moment Curie–Weiss paramagnetism, are consistent with Mott insulator behavior, driven by a combination of strong spinorbit coupling and disorder[38].In this paper, we perform a detailed study on the electronic, magneticand optical properties of theGdRuO$_3$.This compound was synthetized by Alexandra Sinclair and *al* at high pressure [38]and room temperature. In our knowledge, there are not ab initio studies before. So, our calculations are predictive. In this work, we have used the full potential linearized augmented plane wave (FP-LAPW)method within the density functional theory (DFT)[39].We have employed various exchange and correlations approximations: generalized gradient approximation (GGA) [40],GGA+*U*[41] with calculated Coulomb energy(*U*)[42,43],GGA+*U* approach combined with the modified Becke–Johnson (mBJ) potential[44] (mBJ+*U*) and the mBJ+*U* combined with the spin–orbit coupling SOC (relativistic effect) because GdRuO$_3$ contains the strongly correlated Gd−*4f* and Ru-*4d* states.

2. Methodology

The calculations have been performed within DFT implemented in the WIEN2k (0 °K,0 Gpa) code [39]. The atoms have been represented by hybrid full-potential (linear) augmented plane-wave plus local orbitals (L/APW + *lo*) method [45]. In this method wave functions, charge density and potential are expanded in spherical harmonics within no overlapping muffin-tin spheres, and plane waves are used in the remaining interstitial region of the unit cell. First, we have adopted the generalized gradient approximation (GGA-PBE) [40] to optimize crystal structures and investigate electronic structures and magnetism. Because GGA usually underestimates energy band gaps [46], we have used (GGA+*U*) [41] and then (mBJ+*U*): combination of (GGA+*U*) approach with the modified Becke–Johnson (mBJ) approximation for the exchange potential [47]). For the calculations of electronic structures, mBJ+*U*has been shown to improve and produce semiconductor gaps for sp semiconductors, transition metal oxide, insulators and wide-band-gap semiconductors [44, 47–50]. We have taken the electronic correlation into account in this powerful (mBJ+*U*) approach. Because the theoretical semiconductor gaps are improved, much better we can also obtain computational results for the optical properties. We have taken the spin–orbit coupling (SOC) into consideration. Dirac equation for core states allows the calculation of the full relativistic effects while the scalar relativistic approximation is deployed for valence states [51,52]. The cut-off energy is set to (-6 Ry) to separate core states from valance states. The k-mesh size in the first Brillouin zone is a set of 68 k-points equivalent to a 4 x 3 x 4 for 20 atoms orthorhombic structures of GdRuO$_3$. We have constructed harmonic expansion up to l_{max} = 10, set $R_{mt}K_{max}$ = 7, and have used magnitude of the largest vector G_{max} = 12 in charge density Fourier expansions. The Muffin-tin (MT) radii of Gd, Ru, and O atomic spheres are set to 2.4, 1.8 and 1.6 Bohr, respectively. The coulomb potential U_{eff} for the Gd*4f*- and Ru *3d*-orbitals is fixed about 6 eV for both of them. We have studied four configurations of our compound GdRuO$_3$ with the 20-atom crystallographic cell deduced from the atomic positions: anti-ferromagnetic-type A-(AF-A), C-type (AF-C), G-type (AF-G) and the ferromagnetic state (FM).

3. Results and discussion

3.1. Structural properties

The orthorhombic GdRuO$_3$ system investigated here has space group Pnma [53]. The experimental lattice constants are a = 5.8639 Å, b = 7.6005 Å and c = 5.2388 Å [54].Fig. 1. shows the crystal structure of GdRuO$_3$. At first, we have optimized the lattice parameters using the Murnaghan [55] equation of states to the obtained equilibrium lattice constant: the lattice constant a (Å), b(Å), c (Å) the bulk modulus B (Gpa) and its pressure derivative B'. We have also optimized (b/a), (c/a) and ionic positions with GGA. The optimized lattice parameters are summed up in Table 1. The experimental results [38]are also presented for comparison. The optimized volume V got by GGA is about 2% bigger than the experimental one [54]. It can be certainly seen that the lattice constants and volume calculate with GGA are agree with the experimental data [54]. The GGA-optimized also atomic positions, they are summarized in Table 2. After internal structure optimization, the Gd atom occupies the (0.08089192, 0.25, 0.96864528) site, the Ru atom the (0, 0, 0.5) site, the O_1 atom the (0.30679656, 0.05552349, 0.67791686) site, and the O_2 atom the (0.45442967, 0.25, 0.12203532) site in Wyckoff coordinates. These are consistent with the experimental orthorhombic structure [38]. Furthermore, we have calculated the GGA total energies of four different magnetic ordering configurations: the three antiferromagnetic (AFM) and ferromagnetic ones (Fig. 2(a–d)). They are denoted by, A-AFM, C-AFM, G-AFM and FM respectively. The A-AFM structure has been taken as reference for its lowest total energy as shown in Fig. 3.a.This effect is confirmed when we optimized energy versus volume using the GGA + *U* approach (Fig. 3. b). These resultsare not in a good agreement with that obtained by Alexandra Sinclair et al [38]which states that GdRuO$_3$ is paramagnetic between the temperatures 300°K and 2°K. This is logical as long as our calculations are executed by the code WIEN2k (0°K, 0 Gpa). It is clear that the temperature 2°K represents the Neels temperature, which, below it GdRuO$_3$ becomes antiferromagnetic as what we have obtained.

3.2. Calculation of Coulomb energy (U)

We have employed the Madsen and Novak method to treat the set of the atomic-orbitals with dependent potential and associated on-site Coulomb energy (U) and exchange interaction (J) [43]. $U_{eff} = U - J$ substituted for U where (J)is independent of multipolar terms. A rotational invariant form of the full potential calculation has been achieved.

$$E^{orb}(n) = \frac{-U-J}{2}\sum_{\sigma} Tr\,(\hat{n}^{\sigma}.\hat{n}^{\sigma}) \quad (1)$$

where n is the orbital occupation matrix.

In this work, the Gd atom in the $GdRuO_3$ compound has seven $4f$ electrons and we have calculated the effective Coulomb potential (U_{eff}) using:

$$U_{eff} = \left\{\varepsilon_{4f\uparrow}\left[\frac{n+1}{2},\frac{n}{2}\right] - \varepsilon_f\left[\frac{n+1}{2},\frac{n}{2}\right]\right\} - \left\{\varepsilon_{4f\uparrow}\left[\frac{n+1}{2},\left(\frac{n}{2}\right)-1\right] - \varepsilon_f\left[\frac{n+1}{2},\left(\frac{n}{2}\right)-1\right]\right\} \quad (2)$$

The f electrons have been added to the core region and been followed by supercell construction in the light of Madsen and Novak idea [43]. The impurity has been added to the structure as index and a redetermination of the space group was performed. The self-consistent cycle has been thus completed within the spin-polarized calculation. Therefore, the U_{eff} value was calculated to be 6 eV [42]. A similar value was also used for Gd in $GdFeO_3$ by M. Azzouz et al. [29].

Table 1. The lattice parameters optimized with GGA for $GdRuO_3$ in comparison with experimental values

	Config.	b/a	c/a	a (Å)	b (Å)	c (Å)	B(Gpa)	B'	Vol (Å³)
GGA	AFM-A	1.2702	0.8755	5.9834	7.6001	5.2385	203.1389	4.5409	238.2178
GGA	AFM-C	1.2702	0.8901	5.9534	7.5620	5.2991	206.1086	3.9686	238.5634
GGA	AFM-G	1.2702	0.8577	6.0276	7.6563	5.1699	200.3461	4.5324	238.5863
GGA	FM	1.2443	0.8755	6.0319	7.5055	5.2809	198.2539	4.9483	239.0791
Exp. [54]	High.Temp.	-	-	5.8639	7.6005	5.2388	-	-	233.5

Table 2. The atomic positions (x, y, z) optimized with GGA and experimental values for $GdRuO_3$

Atom	Site	x	x exp. [38]	y	y exp. [38]	z	z exp. [38]
Gd	4c	0.08089192	0.08	0.25	0.25	0.96864528	0.98
Ru	4b	0.00000000	0.00	0.00	0.00	0.50000000	0.50
O_1	8d	0.30679656	0.30	0.05552349	0.04	0.67791686	0.68
O_2	4c	0.45442967	0.45	0.25	0.25	0.12203532	0.09

Table 3. The calculated magnetic moments (in Bohr magneton, μ_B) for several sites of the perovskites $GdRuO_3$ using the GGA, GGA+U, mBJ+U and the mBJ+U+SOC approximations.

Magnetic moments	GGA (μ_B)	GGA+U (μ_B)	mBJ+U (μ_B)	mBJ+U+SOC (μ_B)
μGd	6.87068	6.97662	6.85036	6.92146
μ Ru	0.47949	0.67070	0.70521	0.76071
μ O	0.00037	0.00248	0.00312	0.00103
μ interstitial	0.02172	0.00007	0.00032	0.00025
μ Cell	0.11395	0.00000	0.00000	0.00000

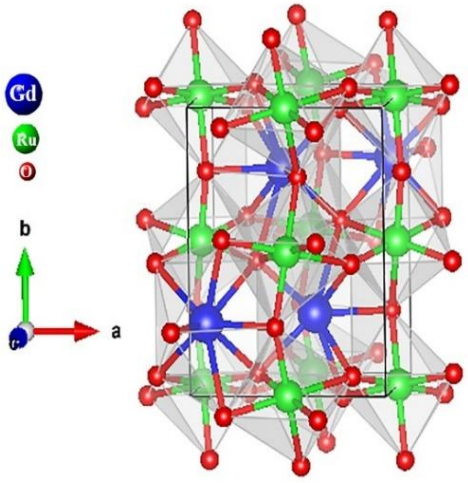

Figure 1. Crystal structure type Pnma of $GdRuO_3$

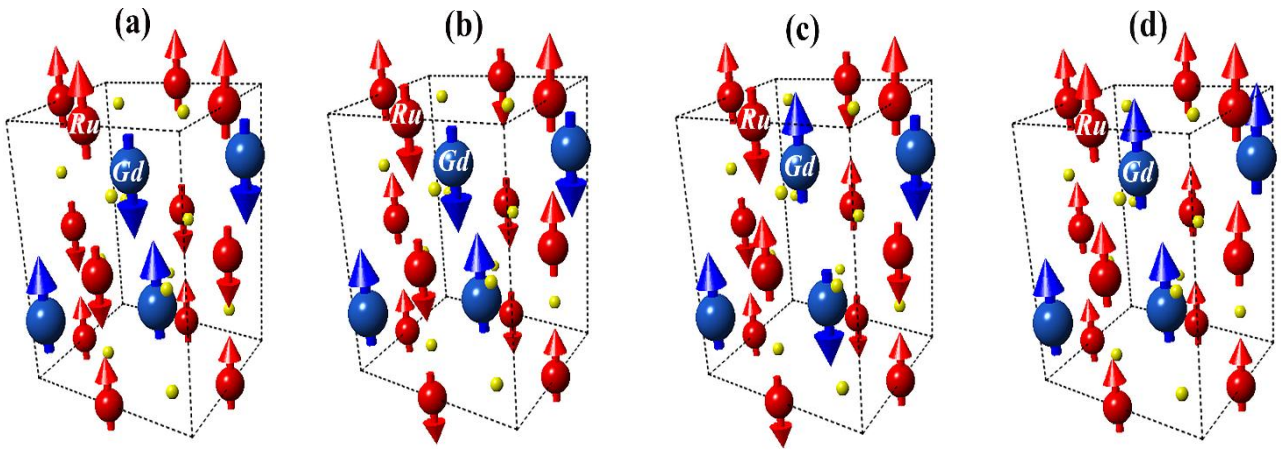

Figure 2. The Crystal structure and magnetic configurations of $GdRuO_3$: (a) A-AFM (b) C-AFM, (c) G-AFM and (d) FM.

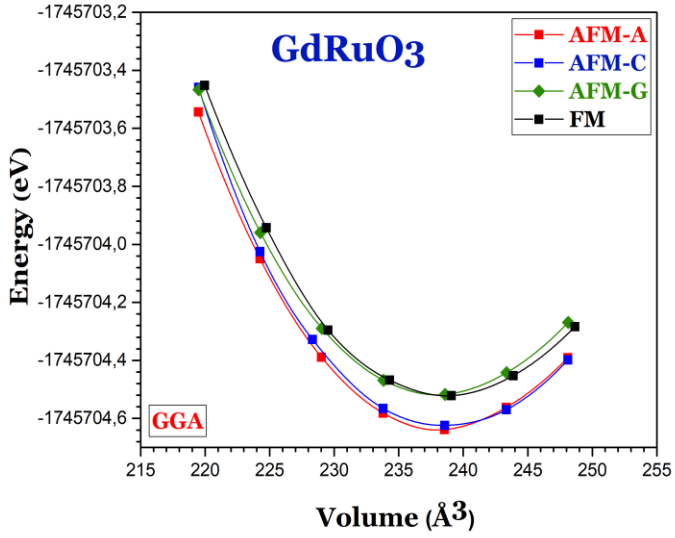

Figure 3.a.The variation of the total energy as a function of the volume of $GdRuO_3$ using GGA approach

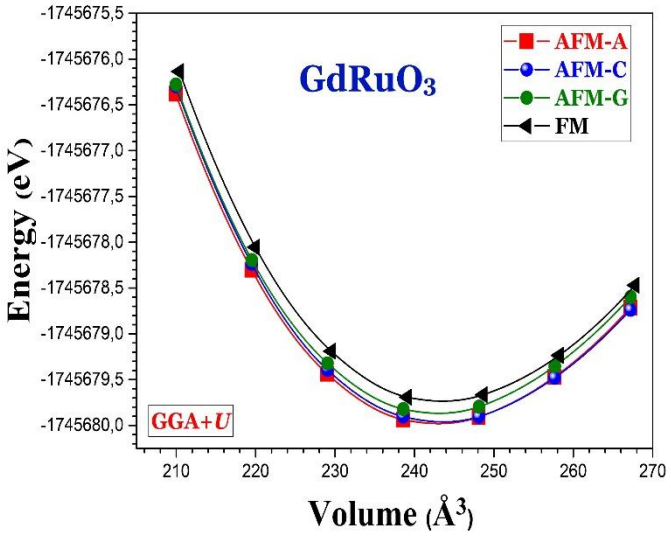

Figure 3.b. The variation of the total energy as a function of the volume of $GdRuO_3$ using GGA+U approach

3.3. Magnetic properties

Table 3 shows the spin effect on the magnetic moment of $GdRuO_3$ compound. This table summarizes the calculated spin magnetic moments for Gd (μ-Gd), Ru (μ-Ru), O(μ-O) atoms, interstitial region (μ-interst) and cell (μ-Cell.) respectively versus the exchange correlation potential. We have investigated a detailed examination of the magnetic properties of $GdRuO_3$. We have used four approximations: GGA, GGA+*U*, MBJ+*U*and MBJ+*U*+SOC. The total magnetic moment which includes the contribution from the interstitial region is equal to zero with all approximations except the GGA (0.11395 μ_B), it is legitimate since we are in magnetic configuration AFM-A. The inclusion of SOCs effect shows a decrease in the Gd moment (6.92146 μ_B) in relation to the GGA+*U* approximation (6.97662 μ_B), this value is not far from the experimental and theoretical ones [56-61]. In Table 3, we can note that with GGA+*U* result, the magnetic moment increases in comparison with the GGA as we know that the *U* value used for the Gd atom is 6 eV. The change in the Gd magnetic moment can be seen via its value that has increased from 6.85036 μ_B got with mBJ+*U* to 6.97662 μ_B obtained with GGA+*U*.In addition, the interstitial moment with GGA is the bigger, its value decreases lightly with the other approximations. We can also see that the magnetic moment of Ru linearly progress, with GGA that the value is 0.47949μ_B, until 0.76071 μ_B obtained with mBJ+*U*+SOC.

3.4. Electronic structures

3.4.1. Band structure and density of states

To better visualize the spin effect on the electronic structure for $GdRuO_3$, we calculate with both GGA+*U*and mBJ+*U* potentials the spin-dependent energy band structures and the densities of states(DOSs) of orthorhombic $GdRuO_3$ between -7 eV and 6 eV. The GGA method is not enough to reproduce the insulating behaviour on the $GdRuO_3$ compound (Fig. 4.a). The three band structures diagram of $GdRuO_3$ along some high-symmetry lines of the orthorhombic Brillouin Zone are shown in Fig. 4.b,Fig. 4.candFig. 4.d where the energy zero of the band structure diagram has been taken at the Fermi level. The conduction band bottom and the valence band top indicate a direct gap at the Y point of the Brillouin zone for orthorhombic $GdRuO_3$. It can be seen that the GGA+*U* semiconductor gap is 1.4369 eV [Fig. 4.b] when the mBJ-calculated semiconductor gap is 2.9039 eV[Fig. 4.c].On the other hand [Fig. 4.d] shows the orthorhombic $GdRuO_3$ spin-resolved energy bands with mBJ+*U*+SOC, the gap obtained is estimated at 3.5355 eV. Here, it is clearly shown, the role performed by mBJ potential and the spin–orbit coupling effect (SOC) in increasing the gap. So, we have just confirmed that $GdRuO_3$ is a wide-band gap semiconductor material [38].Fig.5shows the spin-resolved densities of states (DOSs) of orthorhombic $GdRuO_3$ calculated with mBJ+*U* approach. We can see that the wide valence bands between -6.8 eV and -0.44 eV originate from O-*2p* and Ru-*3p* states with a mixture of some Gd- 3*d*4*f*, and the conduction bands are especially from Ru-*3d* and Gd-*4f* states. Our analysis shows that the Gd and Ru contributions are essentially due to the *f*-Gd and *d*-Ru states respectively, while the 2*p*-O states contribution is not very important. The 4*f*-Gd states are localized at (-6.8 to -2.76 eV) in BV and (3.33 to 6 eV) in BC while the 3*d*-Ru states are at (-6.8 to -0.44 eV) in BV and (2.4 to 6 eV) in BC. The 2*p*-O states are found at (-6.8 to -0.44 eV) in BV and (2.4 to 6 eV) in BC, however Fig. 7.b shows the density of states of orthorhombic $GdRuO_3$ obtained with mBJ+*U*+SOC approximation.

3.4.2. Charge distributions and spin-densities

We have calculated the valence charge density distribution of $GdRuO_3$compound (Fig.6.a) using mBJ+*U* approximation, in order to visualize the nature of chemical bonding linking atoms and to explain the charge transfer between them. The Gd atom is less electronegative than the Ru one: the electronegativity value is respectively 1.2 and 2.2.For this reason, there is a transfer of charge toward the metal atom Ru. We noted that there is an expansion of electronic charge distribution in the oxygen atom sites and a reduction in the Gd atom sites. This rearrangement of charge reflects the electronegativity nature of oxygen and the iconicity of the bond.(Fig.6.a)Shows that Gd–O bonding comes from ionic nature because there are no electrons in common between these atoms. The Ru–O bonding has a covalent character since it had overlapping electron distributions between them. Along the Ru-O bond direction the build-up of bonding charge is very strong because of the domination of the covalent character of the bonding. (Fig.6.b) show the spin-density distribution in (110) plane. Here Ru-cation is considered as the principal contributor because the majority of the magnetic moments is related on its 3d states. The magnetic moment field of Gd is related to the 4*f* states of the $GdRuO_3$ material.

3.5. Optical properties

The energy band structure of a material can be determinate by a great tool: the optical spectroscopy analysis [62, 63]. Fig. 5 shows, for orthorhombic $GdRuO_3$, the mBJ+*U*+SOC calculated curves along the three principal axes of the real ε_1 and imaginary ε_2 parts of the complex dielectric function, the absorption coefficient α, the reflectivity *R*, the refractive index *n*, the extinction coefficient *k*, the optical conductivity $\sigma$and the energy loss function *L*.The complex dielectric function $\varepsilon(\omega)$ is considered as the most important measurable optical quantity because all the other optical constants are derived from it. It is given by the relation

$\varepsilon(\omega) = \varepsilon_1(\omega) + i\varepsilon_2(\omega)$ where $\varepsilon_1(\omega)$ is the real and $\varepsilon_2(\omega)$ the imaginary parts. As the $GdRuO_3$ compound is orthorhombic, the linear optical behaviour can be described by only the imaginary part $\varepsilon_2(\omega)$[64]:

$$\varepsilon_2(\omega) = \frac{4\pi^2 e^2}{m^2\omega^2}\sum_{v,c}\left\{\int_{BZ} d^3k |M_{cv}(k)|^2\, \delta[E_c(k) - E_v(k) - \hbar\omega]\right\} \quad (3)$$

Mcv(k) is the momentum dipole element where integral is performed over the first Brillouin zone. They are also the matrix elements for the direct transitions between the valence band (uvk(r)) and conduction band (uck(r)) states. The electric field is defined by the potential vector δ.

(E_{ck}−E_{vk}) is the corresponding transition energy. The Kramers–Kronig dispersion relation [65]allows to the real part $\varepsilon_1(\omega)$ of the frequency-dependent dielectric function to be deduced from the imaginary part $\varepsilon_2(\omega)$:

$$\varepsilon_1(\omega) = 1 + \frac{2}{\pi} P \int_0^{\infty} \frac{\omega' \varepsilon_2(\omega')}{\omega'^2 - \omega^2} d\omega' \quad (4)$$

(P is the principal value of the integral)

We haven't taken into account scissor shift because of the nonavailability of experimental and theoretical results. The electronic dielectric function spectra calculations (Fig. 5) are performed for energy radiation in the range of 0–30 eV above the Fermi level. It is clear that the compound $GdRuO_3$ presents an anisotropic character in the optical properties for the three crystallographic directions [100], [010] and [001]. The real part of the dielectric function $\varepsilon_1(\omega)$ [Fig. 5(a)] explains widely the electronic polarizability of a material. In the study range, there is a negative region between 10 and 16 eV which means that a part of the electromagnetic wave propagates on the surface of the material (evanescent wave), this explains the increase in reflectivity in this energy range. The other part of this electromagnetic wave propagates inside the material but with a strong attenuation (damped wave) this explains the strong absorption in this range of energy. The static dielectric constant $\varepsilon(0)$ along the three crystallographic directions, got from the real part, are given values: 3.72 for [100], 3.69 for [010], and 3.54 for [001], respectively. The average value of $\varepsilon(0)$ is 3.65. These results clearly confirm anisotropy in the optical properties of orthorhombic $GdRuO_3$. The ratio $\epsilon_1^{yy}(0)/\epsilon_1^{zz}(0)$ is equal to 1.042 for the estimation of the degree of anisotropy. From the zero-frequency limit, they start increasing and reach the maximum value of 6.09 at 5.05 eV for direction [100], 6.06 at 4.61 eV for direction [010], and 5.69 at 5.26 eV for direction [001], respectively. The imaginary part $\varepsilon_2(\omega)$ [Fig. 5(b)] is able to inform us about the absorption behaviour of $GdRuO_3$. The threshold energy of the dielectric function is at 3.5355 eV, it's exactly the value of the band structure gap calculated with mBJ+*U*+SOC: (GGA+*U* approach combined with mBJ and taking into account spin–orbit couplings SOCs effect), very interesting approximation that supply a correct band gap for magnetic semiconductors. The imaginary part also shows that $GdRuO_3$ is anisotropic. The values 7.5, 9.3 and 9.5 eV for directions [100], [010] and [001], respectively, represent the maximum absorption peak. It can be also clearly seen that our compound is totally transparent in the visible range 0-3.5 eV and 15-30 eV. In the energy range of 3.5 – 15 eV, we can note the presence of strong absorption peaks. (Fig.5(c)] shows that $GdRuO_3$ does not absorb light below the band gap value (3.53 eV), thus above this value, it strongly increases, therefore our compound can be considered a highly absorbent material. The reflectivity coefficient R (ω) is presented in Fig. 5(d), the zero-frequency reflectivity values are for [100], [010] and [001] directions respectively 10%, 10% and 9%. The strong minimum reflectivity values are found at 21.25 eV corresponding to 0% for the 3 directions while the strong maximum, are shown at 15.63 eV corresponding to 81% for [100] direction, 15.06 eV to 76% for [010] direction and 15.57 eV to 77% for [001] direction. Fig. 5(e) shows the refractive index values n (ω) which attains a maximum value of 2.5 at 5.14 eV along xx axes of the photon energy. The static refractive index n (0) reaches values 1.93, 1.93 and 1.88, respectively for [100], [010] and [001] directions. The n (0) average value got is 1.91. From the real part of dielectric function, we can obtain the value of the static refractive index using the relation $n(0) = [\varepsilon_1(0)]^{1/2} = (3.65)^{1/2} = 1.91$ which is the same value obtained from Fig. 5(e). The extinction coefficient k (ω) [Fig. 5(f)] automatically describes the electromagnetic waves attenuation within the material. It reflects the maximum absorption at 11.31 eV for [100], 11.22 eV for [010], and 9.84 eV for 001, respectively. The optical conductivity ω) is shown in [Fig. 5(g)]. It starts from 3.53 eV and has similar characteristic with the absorption coefficient α (ω) in Fig. 5(c). [Fig. 5(h)] shows the energy loss function L (ω). It is associate to the energy loss of fast electrons running through the compound from valence band to conduction band and generally wide at the plasmon energy [66]. The outstanding peak in the L (ω) is jointed to the plasmon oscillation resonance. It indicates the excitations of the electronic charge density in the material and is at 16.12 eV for [100] polarization.

3. Conclusion

This is an outlook study of the structural, electronic, magnetic and optical properties of orthorhombic GdRuO3, using the FP-LAPW method. The GGA approach has given the fact that the A-type antiferromagnetic phase of orthorhombic GdRuO3 is more stable in relation to the other magnetic phases. The GGA+U approximation has been used in order to investigate the orthorhombic GdRuO3 behaviour. The Coulomb energy has been calculated theoretically and found to be 6eV while the magnetic moment is found to be 0 μB. The mBJ based study has been conjoined with the GGA+U calculation for giving mBJ+U. This one has substantially enhanced the accuracy and surmount the GGA underestimation of the band gap value.

The valence charge density distribution of GdRuO3 have been calculated using mBJ+U approximation, in order to visualize the nature of chemical bonding linking atoms and explain the charge transfer between them. The spin–orbit coupling (SOC) has been taken into account and has further been used along with the mBJ +U to explore the easy magnetic axis effects on the electronic structure which display a semiconducting band structure where valence band maximum and conduction band minimum happen at point Y. It has supplied a good increase in the energy gap values. The spin–orbit coupling (SOC) has been also used for the investigation on optical proprieties which are presented within results for the real and imaginary parts of the dielectric function and more optical constants. The orthorhombic $GdRuO_3$ is considered to be a wide-band gap semiconductor in accordance with our results and can be used in power electronics and in optoelectronic field.

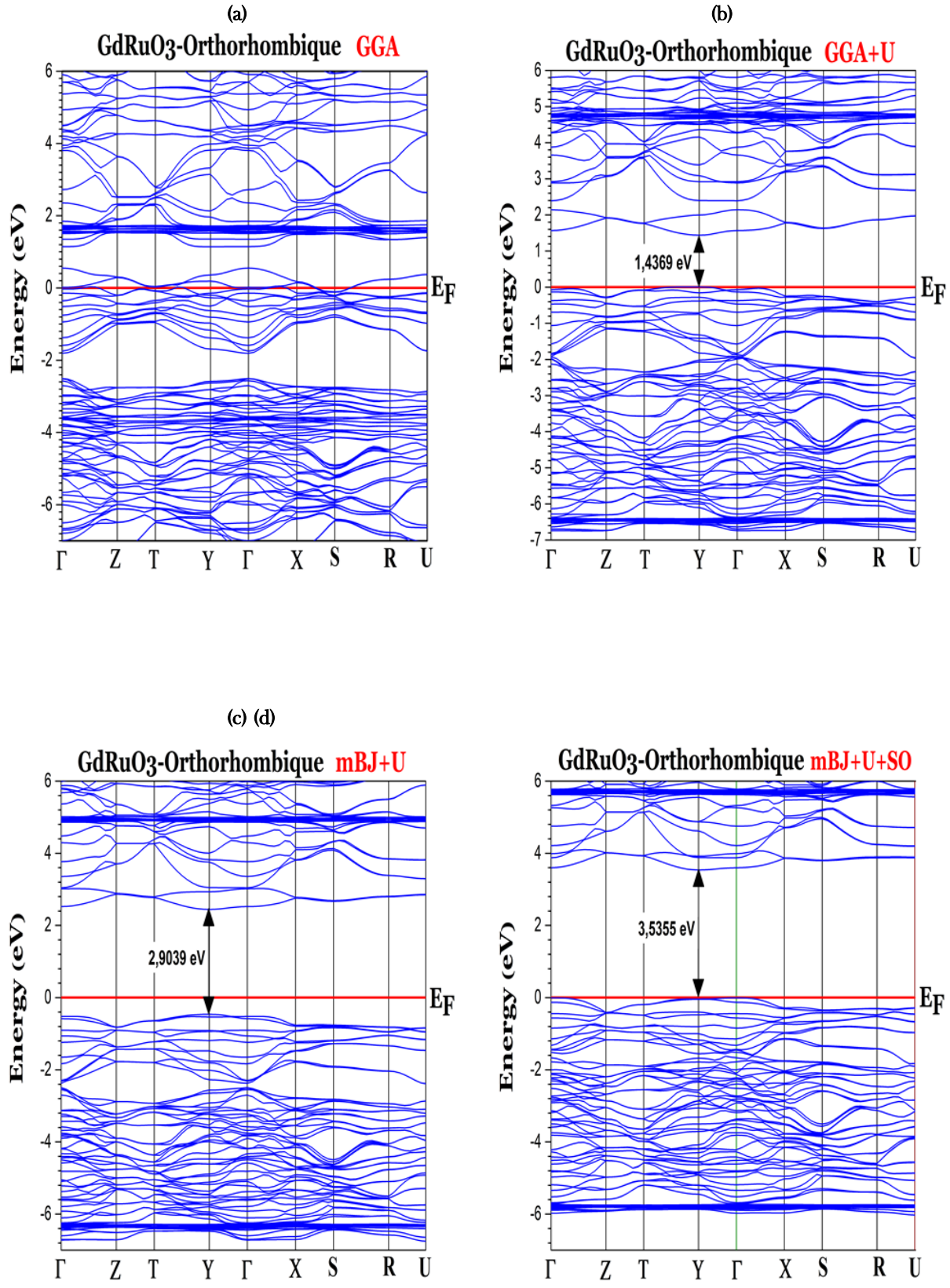

Figure 4. The spin-resolved energy bands of $GdRuO_3$ with (a) GGA, (b) GGA+*U*, (c) mBJ+*U* and (d) mBJ+*U*+SOC

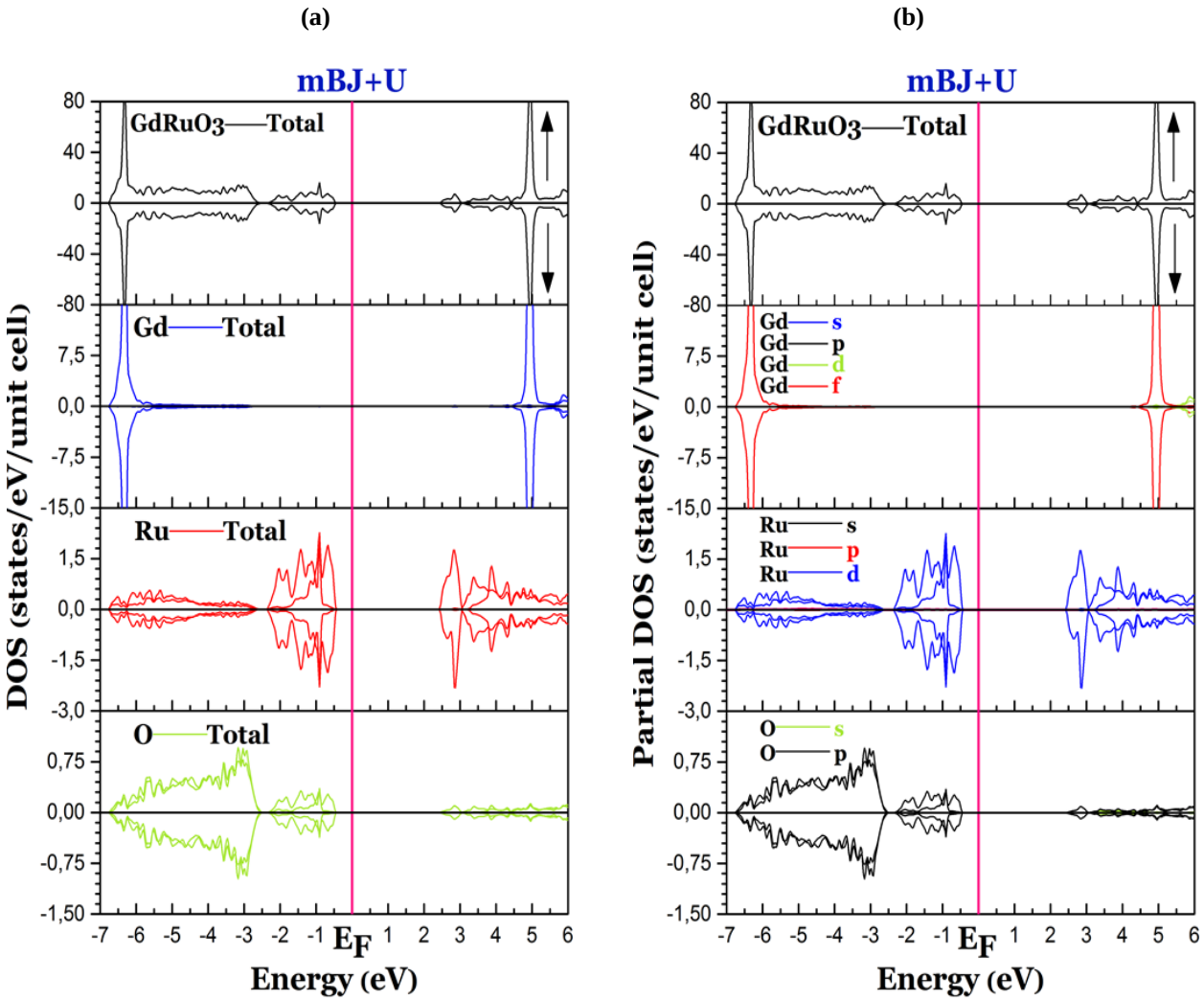

Figure 5. The total and partial DOSs plots of (a) total-$GdRuO_3$, (b) partial-$GdRuO_3$

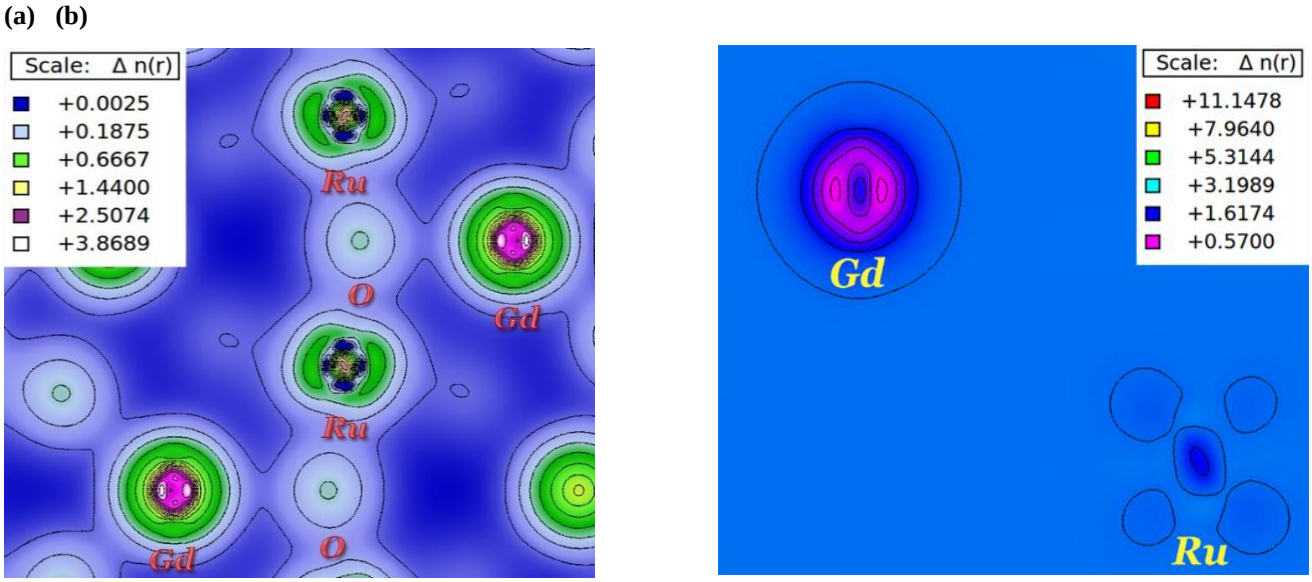

Figure 6. (a) Contour plots of the valence–charge distribution of $GdRuO_3$ compounds in (111) plane, (b) spin-density contours of A-antiferromagnetic $GdRuO_3$ compound, using mBJ+U+SO approach

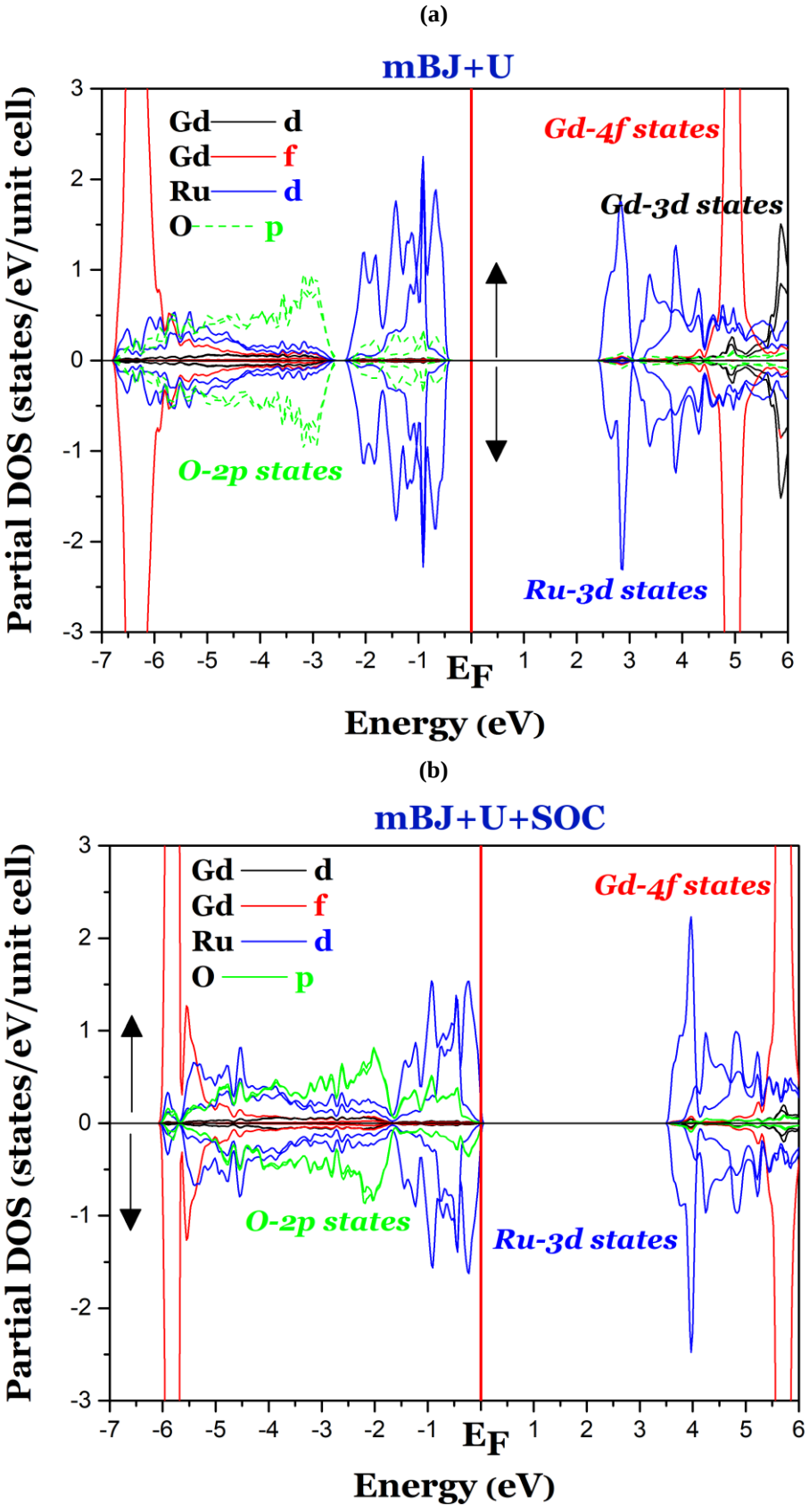

Figure 7. The Gd-*d*,Gd-*f*, Ru-*d*, and O-*p* states with (a) mBJ+*U*, (b) mBJ+*U*+SOC scheme

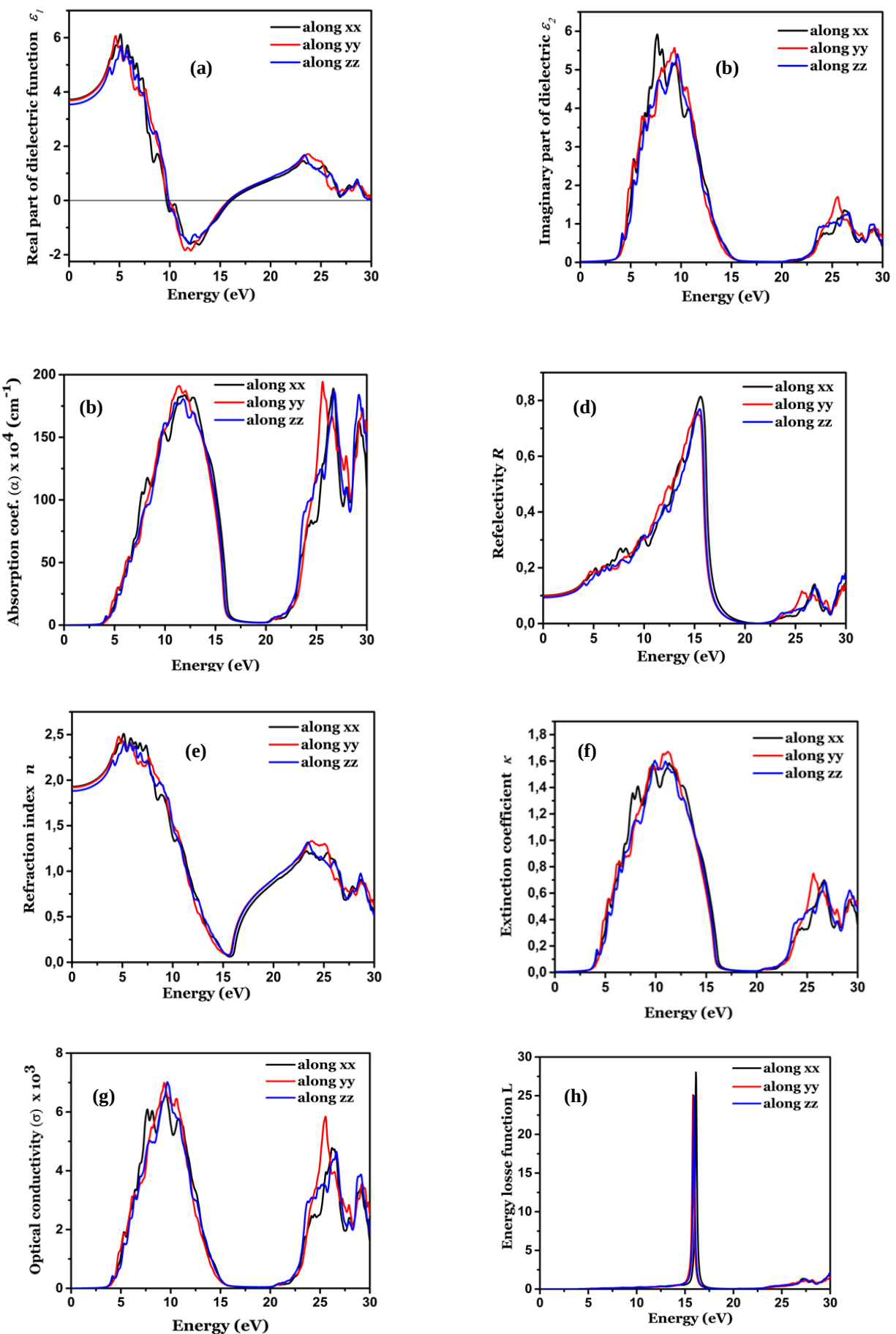

Figure 8. Optical properties of $GdRuO_3$ calculated with mBJ+U+SOC along the three principal axes: (a) real part of dielectric function ε_1, (b) imaginary $\varepsilon_2$part of dielectric function, (c) absorption coefficient α(d) reflectivity R, (e) refractive index n, (f) extinction coefficient k, (g) optical conductivity σ, and (h) energy loss function

References

[1] T. G. Ho, T. D. Ha, Q. N. Pham, H. T.Giang, T. A.Thu Do, N. T. Nguyen, Adv. Nat. Sci. Nanosci. Nanotechnol. 2 (2011) 15012.

[2] T. He, Q. Huang, A. P. Ramirez, Y. Wang, K. A. Regan, N. Rogado, M. A. Hayward, M. K. Haas, J. S. Slusky, K. Inumara, H. W. Zandbergen, N. P. Ong, R. J. Cava, Nature 411 (2001) 54.

[3] K. D. Nelson, Z. Q. Mao, Y. Maeno, Y. Liu, Science (80-.). 306 (2004) 1151.

[4] M. Shang, C. Zhang, T. Zhang, L. Yuan, L. Ge, H. Yuan, S. Feng, Appl. Phys. Lett. 102, (2013) 062903.

[5] Y. Ueda, T. Nakajima, Prog. Solid State Chem. 35 (2007) 397.

[6] K.-I. Kobayashi, T. Kimura, H. Sawada, K. Terakura, Y. Tokura, Nature 395(1998) 677.

[7] R. Terki, H. Feraoun, G. Bertrand,H. Aourag, Phys. StatusSolidi 242(2005) 1054.

[8] S. Cabuk, H. Akkus, A. M. Mamedov, Phys. B Condens. Matter 394 (2007) 81.

[9] R. Ubic, G. Subodh, J. Alloys Compd. 488 (2009) 374.

[10] J. H. Van Santen, G. H. Jonker, J. Phys. Radium 12 (1951) 202.

[11] H. Ding, B. Lin, Y. Jiang, S. Wang, D. Fang, Y. Dong, S. Tao, R. Peng, X. Liu, G. Meng, J. Power Sources 185 (2008) 937.

[12] H. Fu, R. E. Cohen, Nature 403 (2000) 281.

[13] E. Bousquet, M. Dawber, N. Stucki, C. Lichtensteiger, P. Hermet, S. Gariglio, J.-M. Triscone, P. Ghosez, Nature 452 (2008) 732.

[14] Y. Yamasaki, H. Sagayama, N. Abe, T. Arima, K. Sasai, M. Matsuura, K. Hirota, D. Okuyama, Y. Noda, Y. Tokura, Phys. Rev. Lett. 101 (2008) 097204.

[15] L. Chen, H. Fan, M. Zhang, C. Yang, X. Chen, J. Alloys Compd. 492 (2010) 313.

[16] V. Y. Topolov, V. Yu., Solid State Commun. 170 (2013) 1.

[17] C. Le Paven, Y. Lu, H. V. Nguyen, R. Benzerga, L. Le Gendre, S. Rioual, D. Benzegoutta, F. Tessier, F. Cheviré, A. Sharaiha, C. Delaveaud, X. Castel, Thin Solid Films 553 (2014) 76.

[18] Y. Yamada, Y. Kanemitsu, J. Lumin. 133 (2013) 30.

[19] K. Page, T. Kolodiazhnyi, T. Proffen, A. K. Cheetham,R. Seshadri, Phys. Rev. Lett. 101 (2008) 205502.

[20] J.-S. Zhou, J. B. Goodenough, Phys. Rev. Lett. 89 (2002) 087201.

[21] M. Derras, N. Hamdad, Results Phys. 3 (2013) 61.

[22] L. Abbes, H. Noura, Results Phys. 5 (2015) 38.

[23] A. P. Sakhya, A. Dutta, S. Shannigrahi, T. P. Sinha, Solid State Sci. 42 (2015) 37.

[24] M. Mostovoy, J. Phys. Condens. Matter 17 (2005) S753.

[25] Z. Ali, I. Ahmad, B. Khan, I. Khan, Chinese Phys. Lett. 30 (2013) 047504.

[26] A. Fert, Rev. Mod. Phys. 80 (2008) 1517.

[27] I. Žutić, J. Fabian, S. Das Sarma, Rev. Mod. Phys. 76 (2004) 323.

[28] D. Mekam, S. Kacimi, M. Djermouni, M. Azzouz, A. Zaoui, Results Phys. 2 (2012) 156.

[29] M. Azzouz, S. Kacimi, S. Ait Abderahmane, M. Bououdina, A. Zaoui, Mater. Sci. Semicond. Process. 27 (2014) 810.

[30] S. Chettri, D. P. Rai, A. Shankar, R. Khenata, M. P. Ghimire, R. K. Thapa, S. Bin Omran, Int. J. Mod. Phys. B 30 1650078 (2016).

[31] A. Sinclair, J. A. Rodgers, C. V. Topping, M. Míšek, R. D. Stewart, W. Kockelmann, J.-W. G. Bos, J. P. Attfield, Angew. Chemie Int. Ed. 53 (2014) 8343.

[32] R. J. Cava, Dalt. Trans. 0 (2004) 2979.

[33] J. M. Longo, P. M. Raccah, J. B. Goodenough, J. Appl. Phys. 39 (1968) 1327.

[34] G. Cao, S. McCall, M. Shepard, J. E. Crow, R. P. Guertin, Phys. Rev. B 56 (1997) R2916.

[35] C.-Q. Jin, J.-S. Zhou, J. B. Goodenough, Q. Q. Liu, J. G. Zhao, L. X. Yang, Y. Yu, R. C. Yu, T. Katsura, A. Shatskiy, E. Ito, Proc. Natl. Acad. Sci. U. S. A. 105 (2008) 7115.

[36] S. A. J. Kimber, J. A. Rodgers, H. Wu, C. A. Murray, D. N. Argyriou, A. N. Fitch, D. I. Khomskii, J. P. Attfield, Phys. Rev. Lett. 102 (2009) 046409.

[37] F. Denis Romero, S. J. Burr, J. E. McGrady, D. Gianolio, G. Cibin, M. A. Hayward, J. Am. Chem. Soc. 135 (2013) 1838.

[38] A. L. Sinclair, personal communication, 2013.

[39] P. Blaha, K. Schwarz, G. Madsen, D. Kvasnicka, J. Luitz, G. K. H. Madsen, personal communication 2017.

[40] J. P. Perdew, K. Burke, M. Ernzerhof, Phys. Rev. Lett. 77 (1996) 3865.

[41] C. Loschen, J. Carrasco, K. M. Neyman, F. Illas, Phys. Rev. B 75 (2007) 035115.

[42] Sandeep, D. P. Rai, A. Shankar, M. P. Ghimire, R. Khenata,R. K. Thapa, Phys. Scr. 90 (2015) 065803.

[43] G. K. H. Madsen, P. Novák, Europhys. Lett. 69 (2005) 777.

[44] F. Tran, P. Blaha, Phys. Rev. Lett. 102 (2009) 226401.

[45] E. Sjöstedt, L. Nordström, D. Singh, Solid State Commun. 114 (2000) 15.

[46] H. J. Fan, A. S. Barnard, M. Zacharias, Appl. Phys. Lett. 90 (2007) 143116.

[47] D. J. Singh, Phys. Rev. B 82 (2010) 205102.

[48] D. Koller, F. Tran, P. Blaha, Phys. Rev. B 85 (2012) 155109.

[49] S. W. Fan, L. J. Ding, Z. L. Wang, K. L. Yao, Appl. Phys. Lett. 102 (2013) 022404.

[50] A. Ghosh, R. Thangavel, M. Rajagopalan, J. Mater. Sci. 50 (2015) 1710.

[51] A. H. MacDonald, W. E. Picket, D. D. Koelling, J. Phys. C Solid State Phys. 13 (1980) 2675.

[52] J. Kuneš, P. Novák, R. Schmid, P. Blaha, K. Schwarz, Phys. Rev. B 64 (2001) 153102.

[53] J. P. Perdew, P. Ziesche, H. Eschrig, Eds., (1991) 11.

[54] R. D. Shannon, Acta Crystallogr. Sect. A 32 (1976) 751.

[55] F. D. Murnaghan, Proc. Natl. Acad. Sci. U. S. A. 30 (1944) 244.

[56] T. Takeda, Y. Yamaguchi, H. Watanabe, J. Phys. Soc. Japan 33 (1972) 967.
[57] M. Abbate, G. Zampieri, J. Okamoto, A. Fujimori, S. Kawasaki, M. Takano, Phys. Rev. B 65 (2002) 165120.
[58] S. Mathi Jaya, R. Jagadish, R. S. Rao, R. Asokamani, Phys. Rev. B 43 (1991) 13274.
[59] Z. Li, R. Laskowski, T. Iitaka, T. Tohyama, Phys. Rev. B 85 (2012) 134419.
[60] T. Takeda, S.Komura, N.Watanabe, Proc. of the Int. Conf. Japan 1980, ed. H.Watanabe, S.Iida, M.Sugimoto (1981) 385.
[61] I. R. Shein, K. I. Shein, V. L. Kozhevnikov, A. L. Ivanovskii, Phys. Solid State 47 (2005) 2082.
[62] B. Amin, R. Khenata, A. Bouhemadou, I. Ahmad, M. Maqbool, Phys. B Condens. Matter 407 (2012) 2588.
[63] M. Maqbool, B. Amin, I. Ahmad, J. Opt. Soc. Am. B 26 (2009) 2181.
[64] M. Hachemaoui, R. Khenata, A. Bouhemadou, S. Bin-Omran, A. H. Reshak, F. Semari, D. Rached, Solid State Commun. 150 (2010) 1869.
[65] F. Wooten, personal communication, 1972.
[66] P. Nozières, D. Pines, Phys. Rev. 113 (1959) 1254.